Supporting Information

In-situ morphology transformation of bismuth-based catalysts for effective electroreduction of carbon dioxide

Xiaowei An[a], Shasha Li[b, c], Xiaoqiong Hao[b], Xiao Du[d], Tao Yu[a], Zhongde Wang[d], Xiaogang Hao[d], Abuliti Abudula[a], and Guoqing Guan[a, b]*

[a]Graduate School of Science and Technology, Hirosaki University, 1-Bunkyocho, Hirosaki 036-8560, Japan

[b]Energy Conversion Engineering Laboratory, Institute of Regional Innovation (IRI), Hirosaki University, 2-1-3, Matsubara, Aomori 030-0813, Japan.

[c]College of Chemical and Biological Engineering, Taiyuan University of Science and Technology, Taiyuan 030012, China

[d]Department of Chemical Engineering, Taiyuan University of Technology, Taiyuan 030024, China.

*Corresponding author

E-mail: guan@hirosaki-u.ac.jp

Physicochemical Characterizations

The morphology and microstructure of the obtained electrocatalysts were observed by a scanning electron microscope (SEM, Hitachi SU8010) equipped with a Horiba Scientific energy dispersive spectrometer (EDS) analyzer, and the nanostructure was analyzed with a JEM-2100F transmission electron microscope (TEM, JEOL, Japan). The crystalline structures of the electrocatalysts were determined by X-ray diffraction (XRD, RigakuSmartLab X-Ray Diffractometer) using a Cu-Kα (λ=1.5405 Å) radiation source. The surface compositions and their valence states on the catalyst were characterized by using a X-ray photoelectron spectroscopy (XPS) (Thermo ESCALAB 250XI).

Electrochemical Characterizations

Linear sweep voltammetry (LSV) was carried out in a potential range of -0.8 to -2 V at a scan rate of 10 mV s^{-1} in either N_2 or CO_2-saturated 0.1 M $KHCO_3$ solutions. Electric double layer capacitance was determined by cyclic voltammetry (CV) measurements at various scan rates (40, 80, 120, 160, 200 mV s^{-1}) in N_2-saturated 0.1 M $KHCO_3$ solution. The double layer capacitance of each electrode was calculated using Equation (1):

$$J=C\times dV/dt \quad (1)$$

where J is the current density, C the capacitance, and dV/dt the scan rate.

Electrochemical impedance spectroscopy (EIS) was performed within a frequency range of 0.01 Hz - 0.1 MHz in a CO_2-saturated 0.1 M $KHCO_3$ solution at -1.2 V.

Calculation of the Overpotential

The overpotential in Tafel curve was calculated as the difference between the cathodic potential and the standard (equilibrium) reduction potential ($\eta = |E_{Cd} - E_{eq}|$). The standard reduction potential for converting CO_2 into HCOOH in aqueous 0.1 M $KHCO_3$ electrolyte solution is -0.09 V *vs.* RHE.[1] The formula used to convert potentials vs. Ag/AgCl (1M) to vs. RHE is: E vs. RHE = E (V) vs. Ag/AgCl (saturated KCl) + 0.198 (V) + 0.059 (V) × pH (6.8).

Calculation of the electrochemically active surface area (ECSA)

The ECSA of electrode was calculated from the double layer capacitance (C_{dl}) according to equation 2:

$$ECSA = C_{dL}/\alpha \quad (2)$$

where α is the specific capacitance of the sample or the capacitance of an atomically smooth planar surface of the material per unit area under identical electrolyte conditions.

Product Analysis

Gas products were analyzed with a gas chromatography (GC, Agilent 7890A GC system, USA), by which CO and H_2 were detected with two thermal conductivity detectors (TCD), respectively. Liquid products were analyzed using a Shimadzu high performance liquid chromatography (HPLC) equipped with SPD-20AV and RID-10A detectors. Supelcogel C610-H (30 cm×7.8 mm, Sigma) and H_3PO_4 (0.05 %) solution were used as the column and mobile phase, respectively. The temperature of the oven CTO-20A was set at 40 ºC. The faradaic efficiency of HCOOH, CO or H_2 was calculated as follows:

$$\text{Faradaic efficiency} = 2F \times n/Q \quad (3)$$

where F is the faraday constant, n the total amount of products (in moles), and Q the amount of total charge (in Coulomb).

DFT Computational Details

Bi and $Bi_2O_2CO_3$ crystal structures with the ICSD numbers of 053797 and 036245 respectively were imported. All the models were optimized by using the spin-polarized DFT computations with an all-electron method by the DMol3 module in Materials Studio software.[4-5] The electron exchange-correlation functions of generalized gradient approximation (GGA) and Perdew-Burke-Ernzerhof (PBE), and basis set of double numerical plus polarization (DNP) were used for these calculations.[2] Specifically, the van der Waals correction was employed by using DFT-D^3 to accurately describe the long-range electrostatic interactions. The solvent effects were also

applied by using a conductor-like screening model (COSMO)[4] with the H_2O dielectric constant of 78.54.

Other specific parameters selected in this study were consistent with the data reported in the literature.[5, 6] In detail, the convergence criterion was selected as 10^{-6} a.u. with the maximum force of 0.002 a.u. $Å^{-1}$ and the maximum displacement of 0.005 Å. The k points were set as 5×5×1 by using the Monkhorst-Pack method.[7] The real-space global orbital cutoff radius was chosen as 4.7 Å in all the computations to ensure high quality.

The free energy of electrochemical reduction of CO_2 was calculated based on a computational hydrogen electrode (CHE) model,[8] in which the chemical potential of a proton/electron ($H^+ + e^-$) in solution is equal to the half chemical potential of a gas-phase H_2. The adsorption energy of adsorbate was defined as:

$$E_{ad} = E_{surface\text{-}adsorbate} - E_{surface} - E_{adsorbate} \quad (4)$$

where $E_{surface\text{-}adsorbate}$, $E_{surface}$, and $E_{adsorbate}$ are the DFT total energy for the adsorbate on the surface, surface, and adsorbate itself, respectively.

The change in Gibbs free energy (ΔG) was evaluated by the following equation:

$$\Delta G = \Delta E + \Delta E_{zpe} - T\Delta S - neU \quad (5)$$

where the ΔE, ΔE_{zpe} and ΔS are the differences of DFT energy, zero point energy and entropy between products and reactants, respectively. T was set at 298.15 K in this work. E_{zpe} can be obtained by the vibrational frequency analysis over all normal modes ν ($E_{zpe} = 1/2\Sigma\hbar\nu$). The entropies of the free molecules (CO, CO_2, HCOOH, H_2, and H_2O) were obtained from the NIST database. The configurational entropy in the adsorbed state was neglected by fixing the surfaces according to the way in most of the literatures.[9-11] U is the applied potential vs. normal hydrogen electrode (NHE), e is the elementary charge transferred and n is the number of proton-electron pairs transferred.

Investigation of morphology transformation conditions

In order to confirm the formation mechanism of $Bi_2O_2CO_3$ nanosheets, a series of treatment processes were performed and the morphology of electrode surface was observed the by SEM. Because the *in-situ* treatment process consisted of two steps, the first was electrochemical treatment step, and the second was the dry step in the air. In order to confirm whether two steps were necessary, a set of parallel experiments were performed. Four Bi/Cu foam electrodes were treated with the following four different treatment methods and then the surface morphologies were observed.

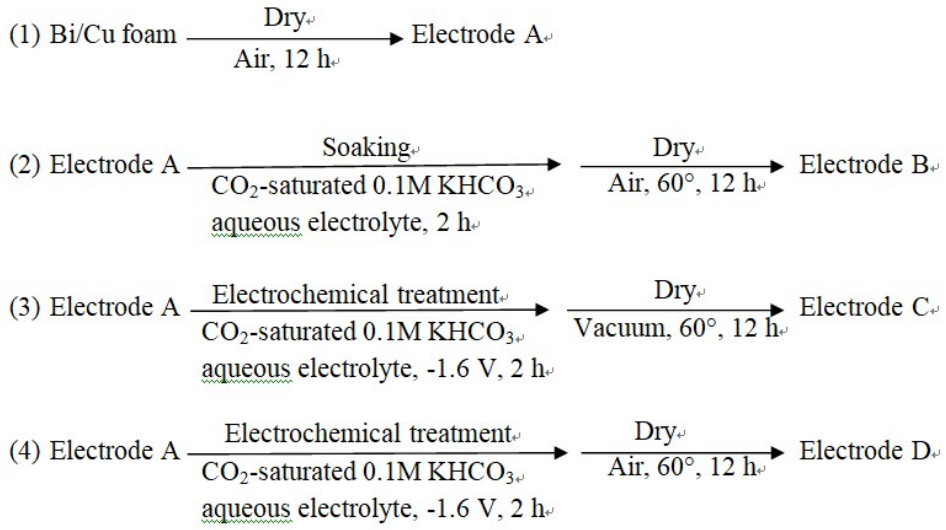

The obtained SEM images for the surfaces of four electrodes are shown as follows:

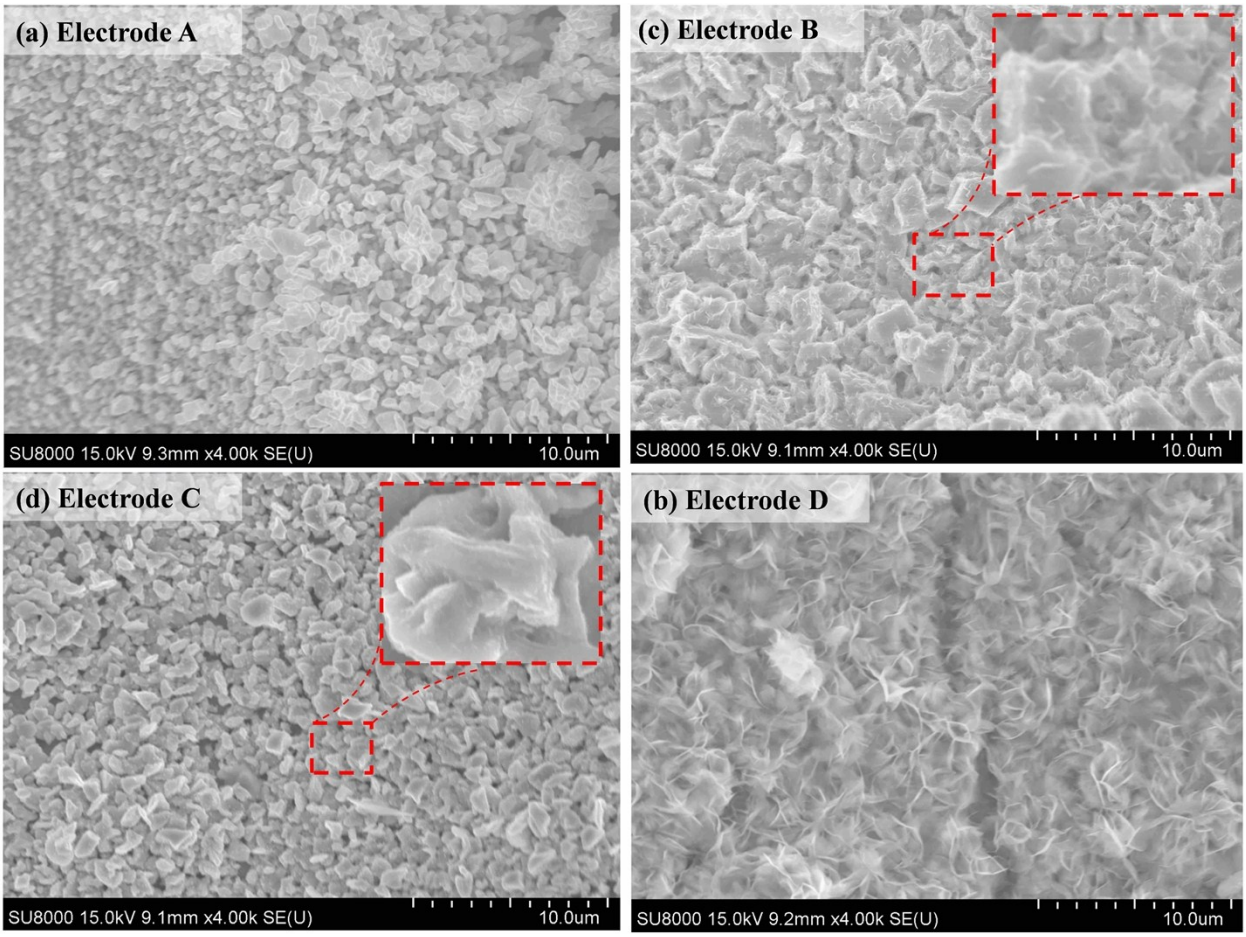

Fig. S1 SEM images of surfaces of electrode (a) A, (b) B, (c) C and (d) D.

The freshly prepared Bi/Cu foam electrode was directly dried in the air as the initial electrode A for comparison. The two same electrodes of A were only soaked and electrochemically treated in the electrolyte for 2 hours using the above methods, respectively, and then the two electrodes were taken out and exposed to the air for 12 hours, which are called as electrodes B and D respectively. As shown in the Fig. S1a, b and d, significant change was observed for the electrochemically treated electrode D, and the electrodes without electrochemical treatment had only a slight surface change. Another electrode A was electrochemically treated at first and

then placed in a vacuum oven to avoid contact with air to obtain electrode C. As shown by the SEM image, the electrode surface became rough after the electrochemical treatment.

For the electrode B, since there was no electrochemical treatment process, in this case, as reported in the literature, $Bi_2O_2CO_3$ was slowly formed on the electrode by reaction with the electrolyte ($KHCO_3$) remained on the surface as follows.[12]

$$4Bi + 3O_2 + 2H_2O \rightleftharpoons 4BiO^+ + 4OH^- \quad (6)$$

$$2BiO^+ + CO_3^{2-} \rightleftharpoons Bi_2O_2CO_3 \quad (7)$$

As such, even without the electrochemical treatment, the electrode B still underwent a slight morphological transformation (Fig. S1b).

For the electrode C, as reported in the literature, in the process of electrochemical reduction of CO_2, some reactions like equations of 8-10 may occur on the surface of the electrode at first, thereby accumulating a large amount of OH^- on the surface, resulting in local alkalinity.[13]

$$CO_2 + H_2O + 2e^- \rightleftharpoons HCOO^- + OH^- \quad (8)$$

$$CO_2 + H_2O + 2e^- \rightleftharpoons CO + 2OH^- \quad (9)$$

$$2H_2O+4e^- \rightleftharpoons H_2+2OH^- \quad (10)$$

$$Bi^{3+}+ OH^- \rightleftharpoons Bi(OH)_3 \quad (11)$$

$$2Bi(OH)_3+CO_2 \rightleftharpoons Bi_2O_2CO_3+3H_2O \quad (12)$$

Then, the OH^- reacted with the Bi^{3+} present on the surface of the electrode to form $Bi(OH)_3$. Since electrode C was directly dried in a vacuum oven after electrochemical treatment, the further reaction between $Bi(OH)_3$ formed on the surface and CO_2 in the air was avoided. In this case, since the solubility of CO_2 in the aqueous solution is very low, only a small amount of $Bi_2O_2CO_3$ could be formed on the electrode surface. As a result, the formation of $Bi(OH)_3$ and a small amount of $Bi_2O_2CO_3$ species resulted in a rough electrode surface but without further morphological transformation (Fig. S1c).

However, for the electrode D, after electrochemical treatment, since the electrode was directly exposed to air, $Bi(OH)_3$ should react with CO_2 in the air to form $Bi_2O_2CO_3$ as indicated by the equation 12. Meanwhile, after the electrochemical treatment, the rough electrode surface could also accelerate the conversion of the metal Bi to $Bi_2O_2CO_3$ as indicated by the equations of 6-7. These caused its surface to be transformed to petal-shaped $Bi_2O_2CO_3$ nanosheets completely (Fig. S1d). In addition, it should be noted that, in order to make the morphological transformation more fully, the electrolyte remaining on the electrode surface after electrochemical treatment should not be washed away.

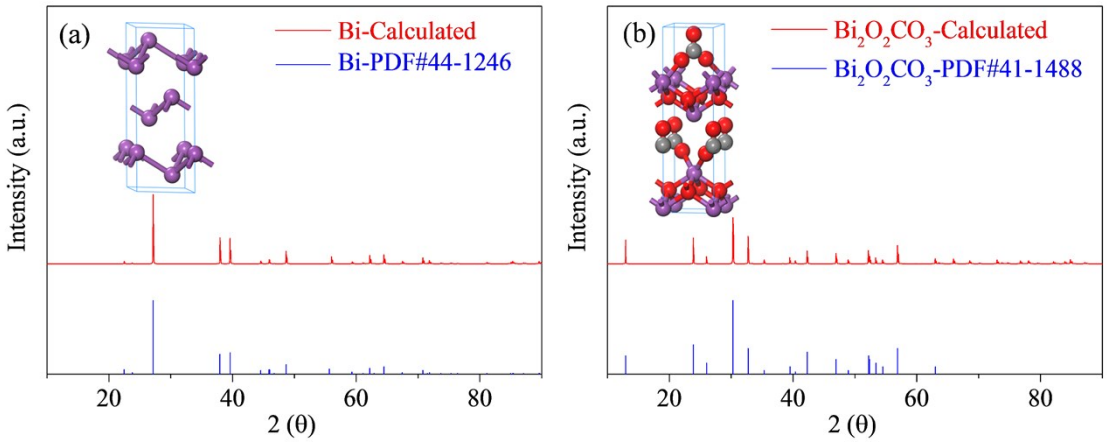

Fig. S2 Calculated XRD patterns of (a) Bi and (b) $Bi_2O_2CO_3$ crystalline structures based on the models and compared with the standard PDF cards from ICDD database.

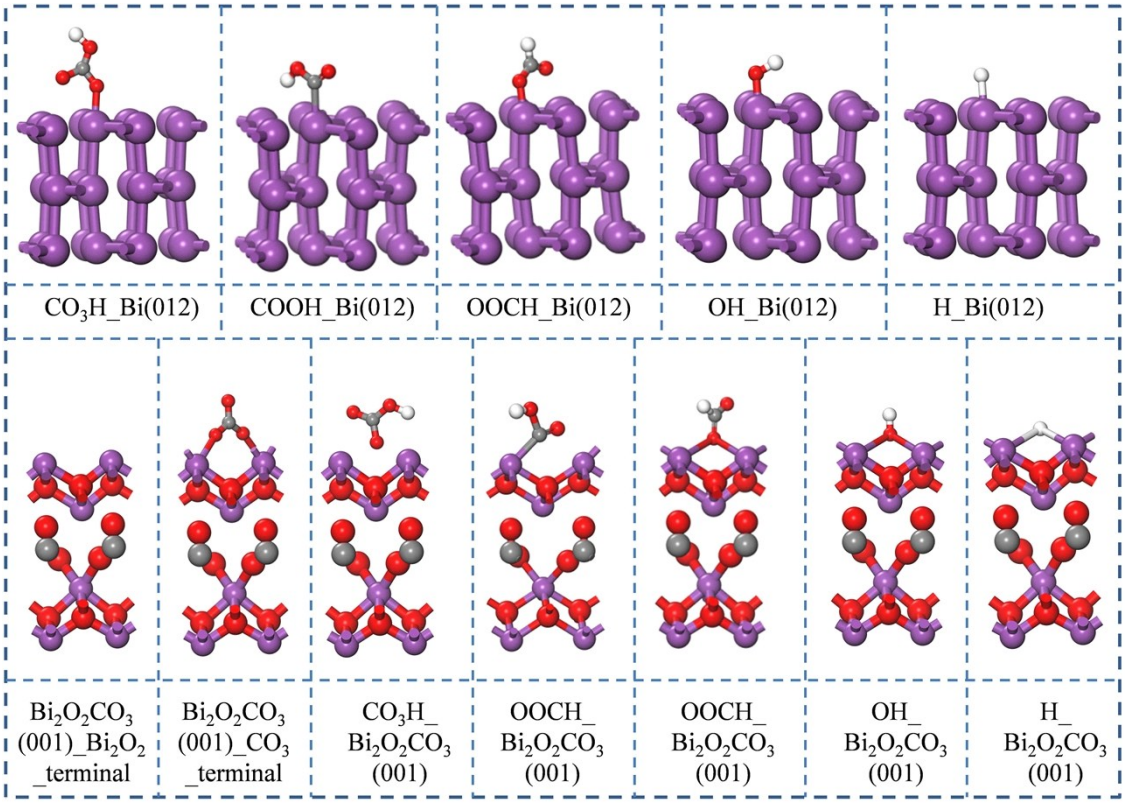

Fig. S3 Optimized structures of different intermediates on the Bi (012) and $Bi_2O_2CO_3$ (001) facets.

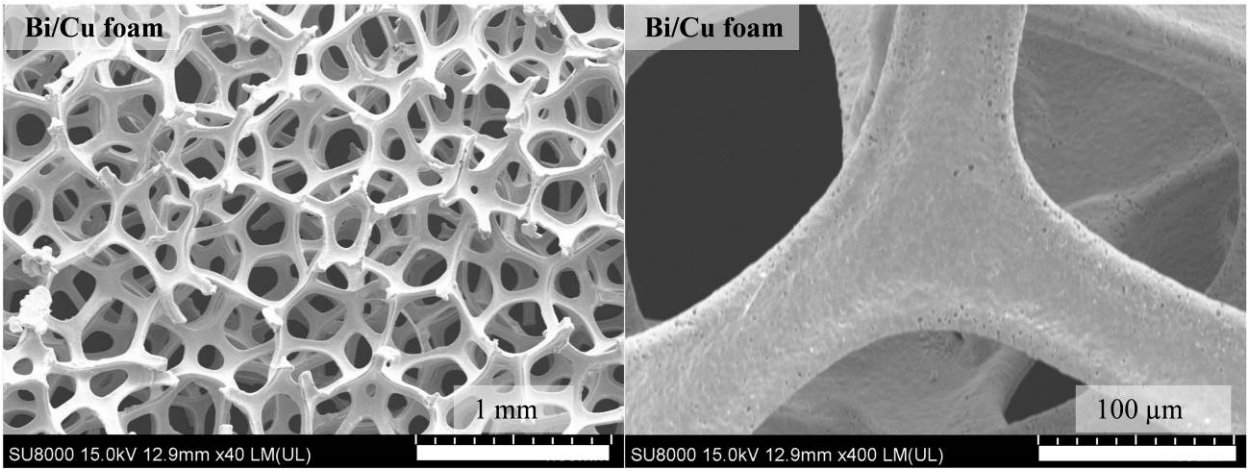

Fig. S4 SEM images of Cu foam with different scales.

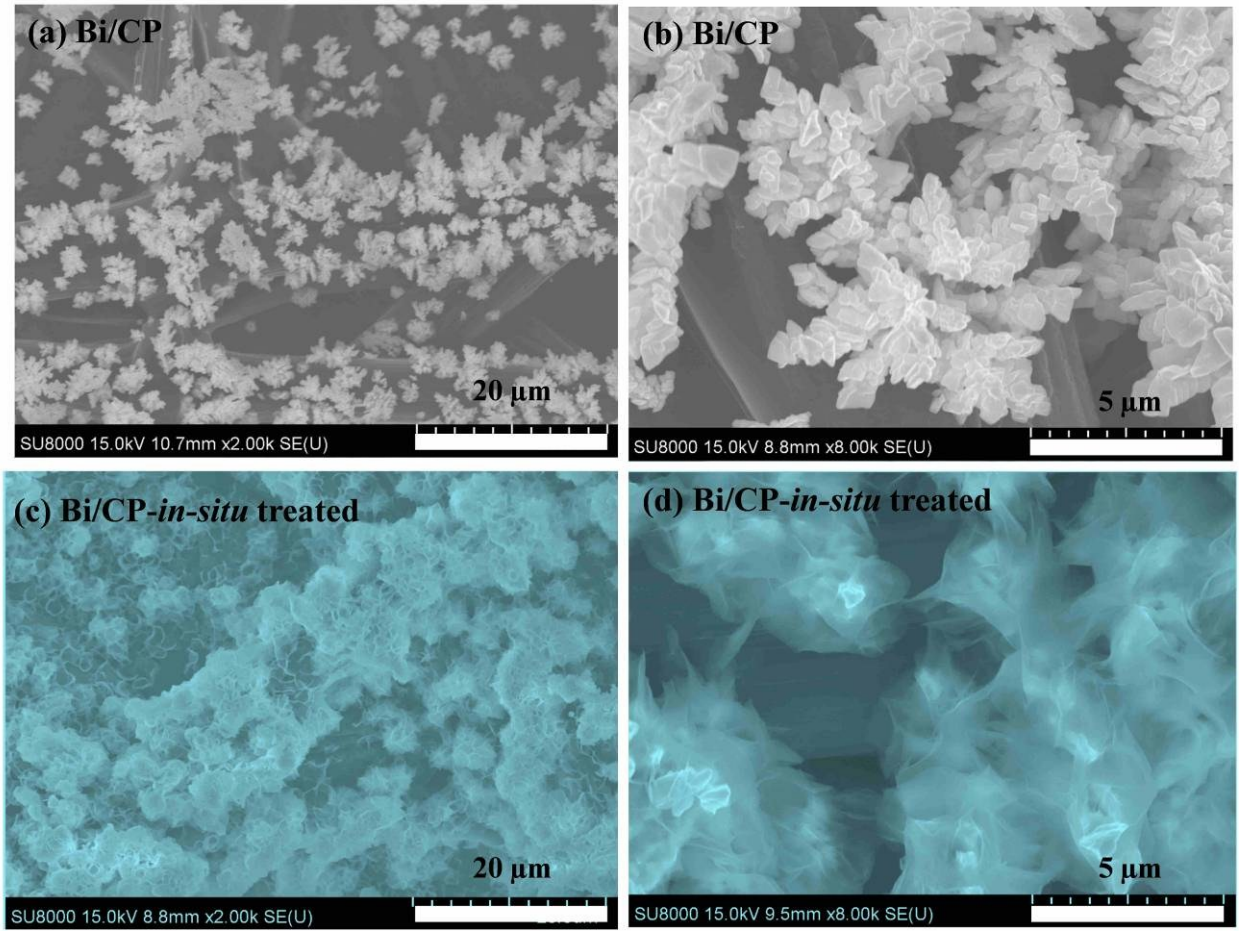

Fig. S5 SEM images of Bi/CP electrode (a, b) before and (c, d) after the *in-situ* treatment.

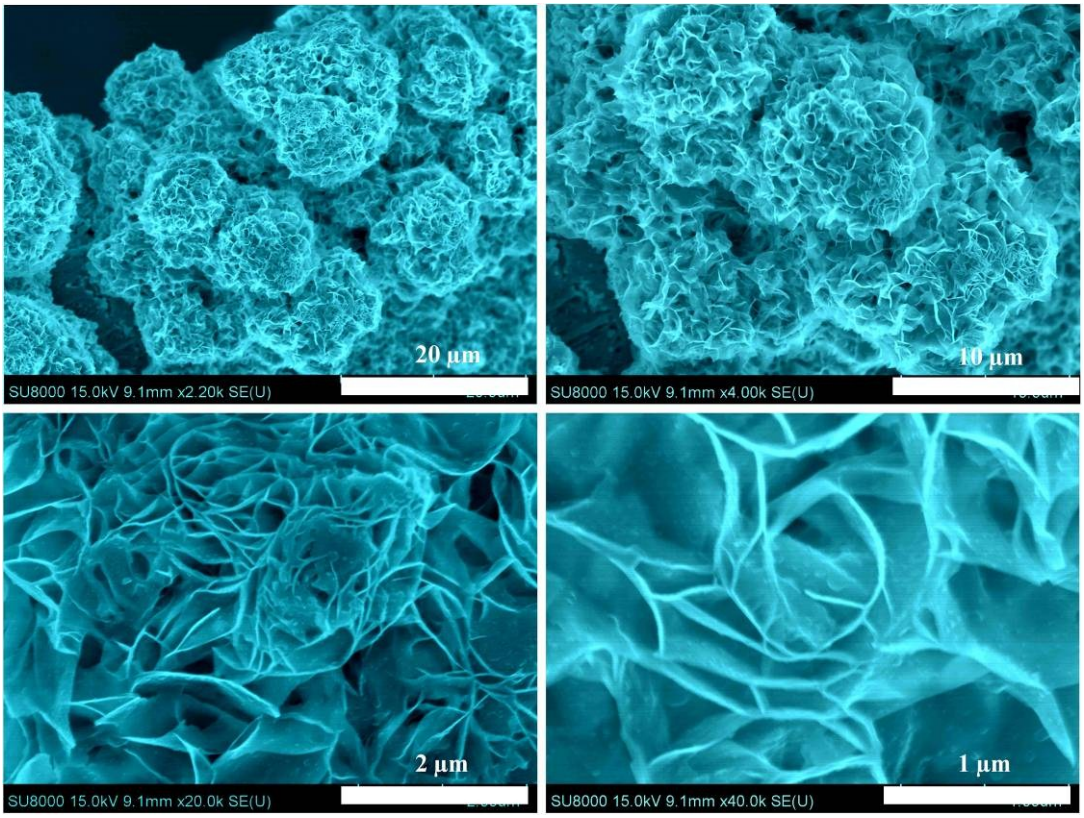

Fig. S6 SEM images of Bi/Cu foam-*in situ* treated electrode with different magnification scales.

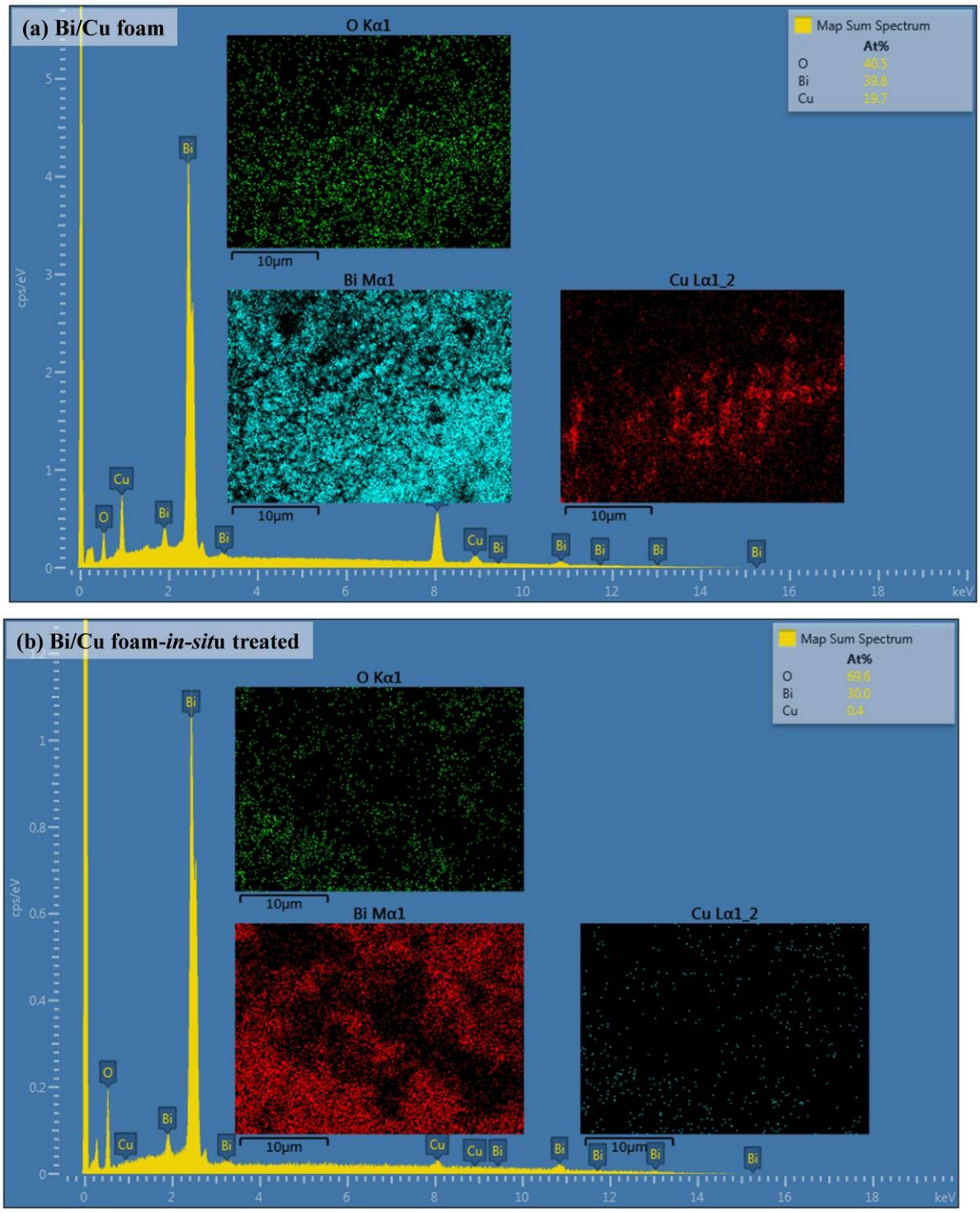

Fig. S7 EDS analysis results of (a) Bi/Cu foam and (b) Bi/Cu foam-*in-situ* treated electrodes.

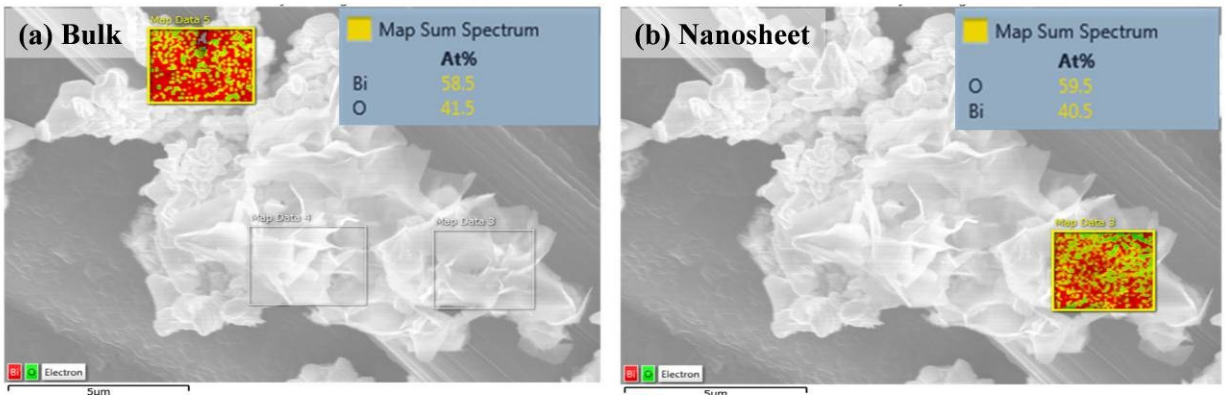

Fig. S8 EDS analysis results of Bi/CP electrode for (a) bulk and (b) nanosheet structures. It can be seen that the area where the morphological transformation has taken place has a higher oxygen content.

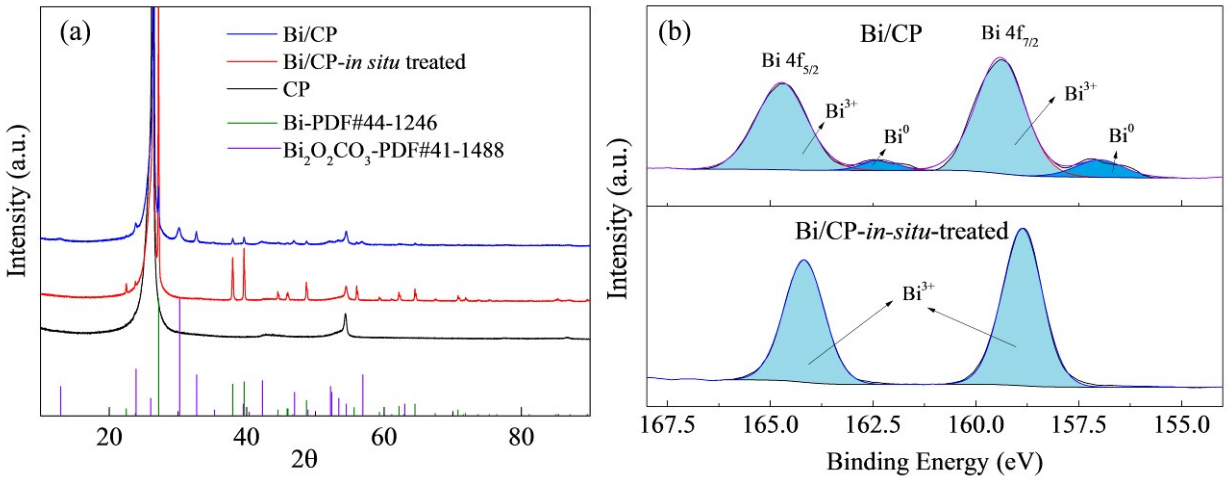

Fig. S9 (a) XRD patterns and (b) high-resolution Bi 4f XPS spectra of Bi/CP and Bi/CP-*in-situ* treated electrodes.

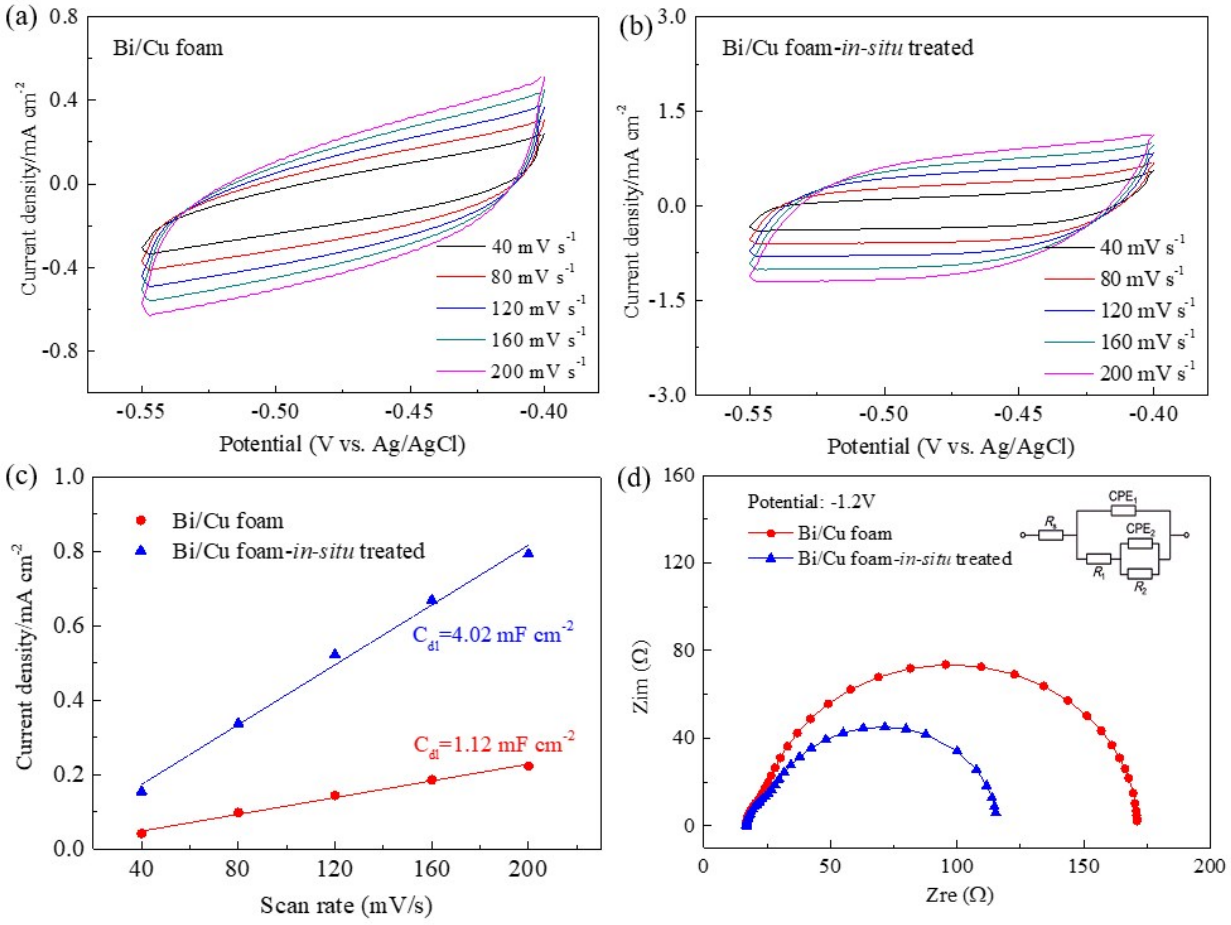

Fig. S10 (a, b and c) Determination of electrochemical double layer capacitance and (d) electrochemical impedance spectroscopy (EIS) tests for Bi/Cu foam and Bi/Cu foam-*in-situ* treated electrodes.

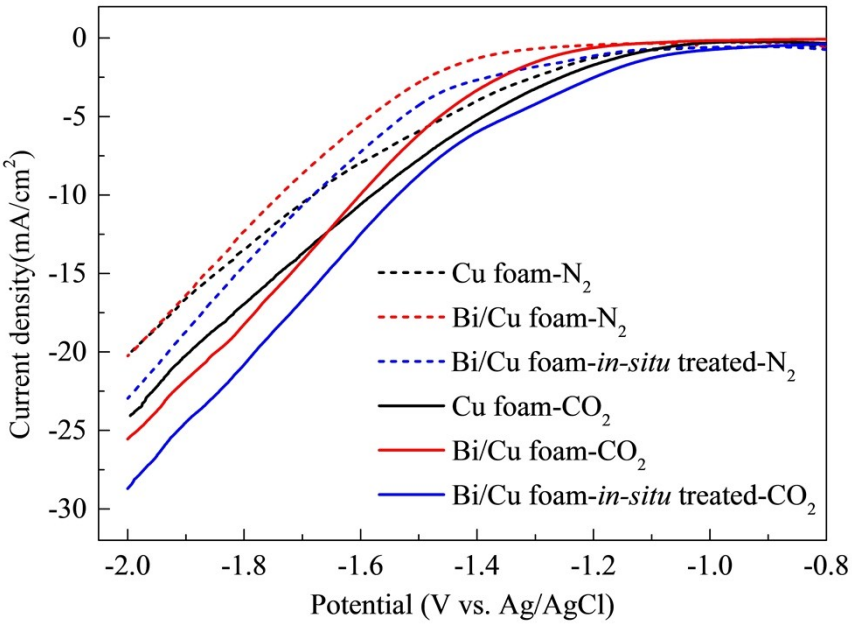

Fig. S11 Linear sweep voltammetry (LSV) curves of the Cu foam, Bi/Cu foam and Bi/Cu foam-*in-situ* treated electrodes in either N_2-saturated (dashed) or CO_2-saturated (solid) 0.1 M $KHCO_3$ solutions at a scan rate of 10 mV s^{-1}.

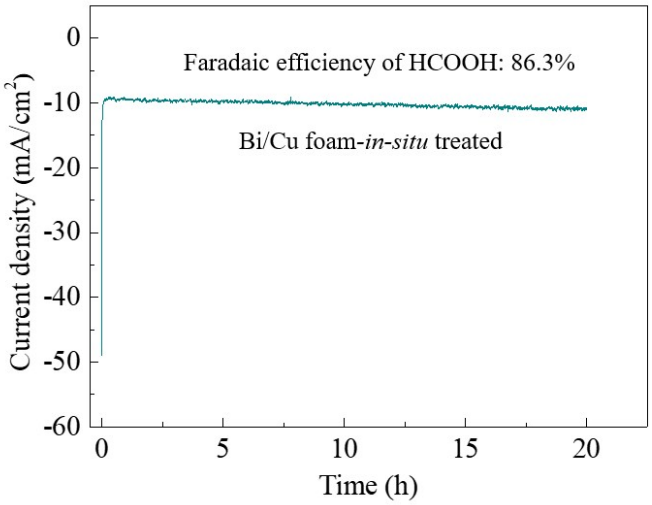

Fig. S12 The stability test of the Bi/Cu foam-*in-situ* treated electrode continuously operated at -1.6 V in a CO_2 saturated 0.1 M $KHCO_3$ solution (without refreshing) for 20 h.

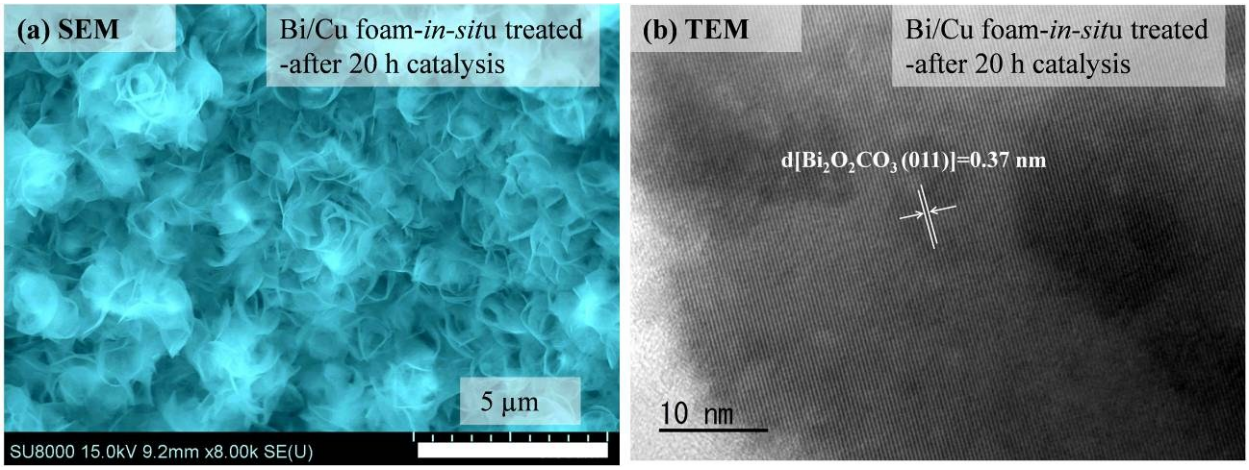

Fig. S13 (a) SEM and (b) TEM images of Bi/Cu foam-*in-situ* treated electrode after 20 h electrocatalysis.

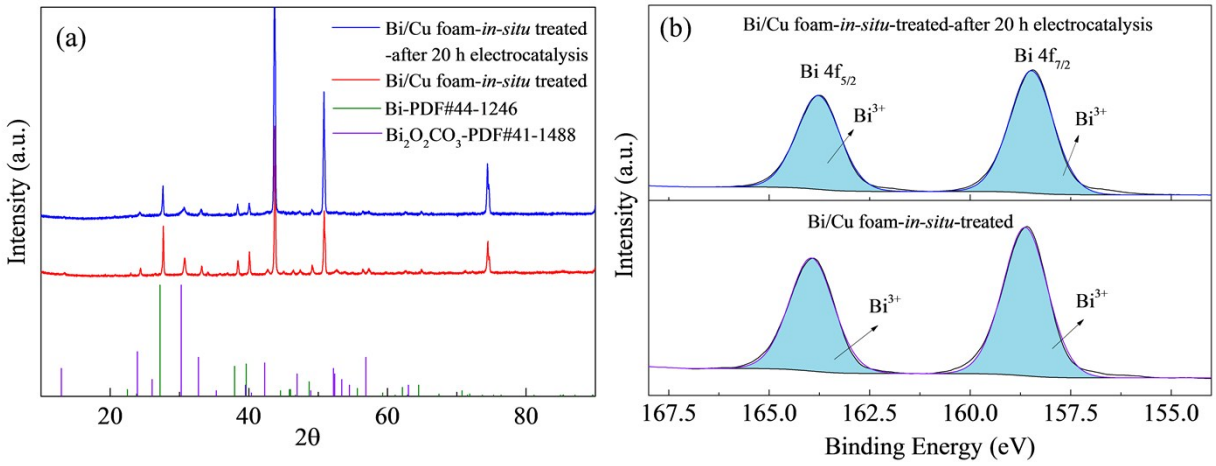

Fig. S14 (a) XRD patterns and (b) high-resolution Bi 4f XPS spectra of Bi/Cu foam-*in-situ* treated electrode before and after 20 h electrocatalysis.

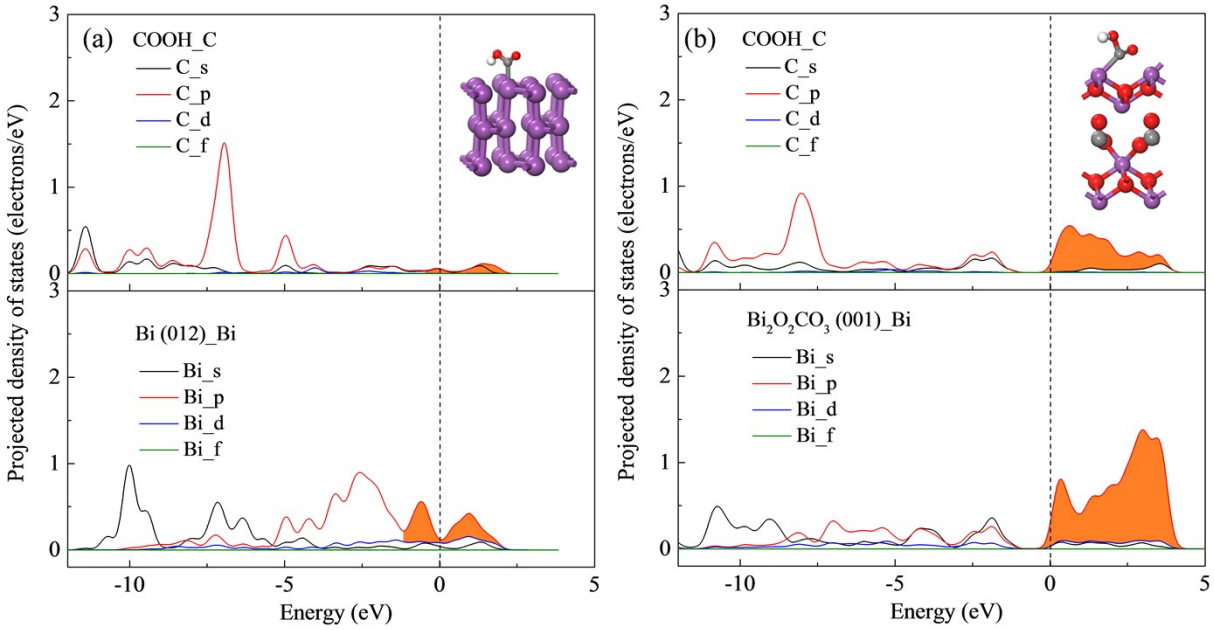

Fig. S15 Projected density of states (PDOS) of C of *COOH intermediate and Bi atoms on the (a) Bi(012) and (b) $Bi_2O_2CO_3$(001) facets. The Fermi level is denoted with a red dashed line.

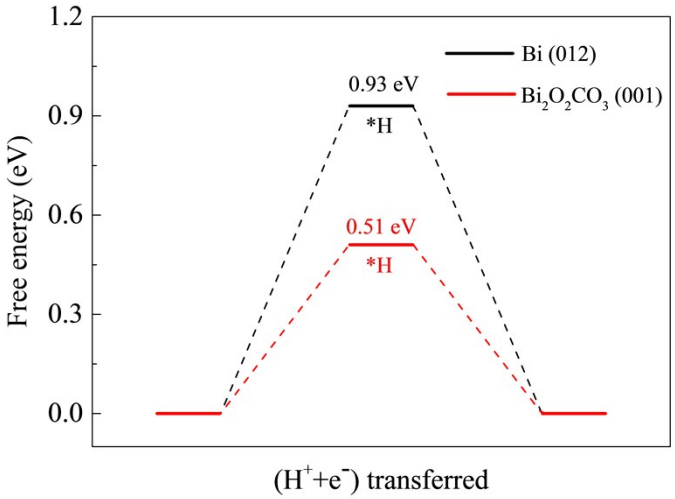

Fig. S16 Calculated free energy diagrams for the H_2 evolution on Bi(012) and $Bi_2O_2CO_3$(001) facets.

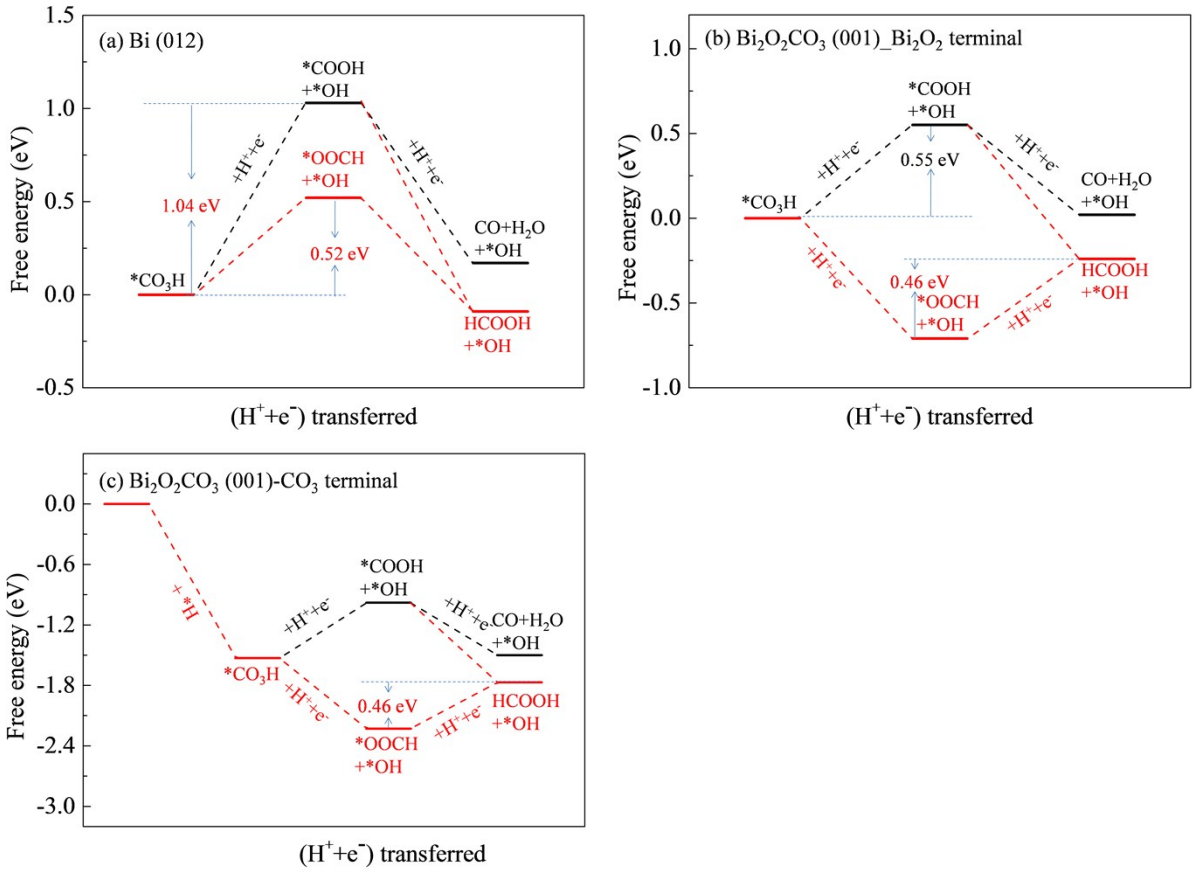

Fig. S17 Calculated free energy diagrams for the electroreductions of *HCO_3 to HCOOH and CO on (a) Bi(012) and (b) $Bi_2O_2CO_3$(001)_ Bi_2O_2 terminal and (c) $Bi_2O_2CO_3$(001)_CO_3 terminal facets. For $Bi_2O_2CO_3$, its (001) crystal plane has two terminals, the $Bi_2O_2CO_3$(001)_CO_3 terminal can be combined with a *H to form *CO_3H and then further reduced.

Table S1 The quantitative results of XPS spectra for the Bi/Cu foam electrode before and after *in-situ* treatment.

Species	At %	
	Bi/Cu foam	Bi/Cu foam-*in-situ* treated
Bi	43.36	28.41
O	52.91	69.32
Cu	3.73	2.27

Table S2 The lattice spacings of Bi and $Bi_2O_2CO_3$.

Bi		$Bi_2O_2CO_3$	
Facet	Lattice spacing d (Å)	Facet	Lattice spacing d (Å)
003	3.954	002	6.841
101	3.737	011	3.720
012	3.280	004	3.420
104	2.369	013	2.952
110	2.273	110	2.734
015	2.032	020	1.933

Table S3 j_{HCOOH} at -1.2 V (vs. Ag/AgCl, -0.6 V vs. RHE), measured double layer capacitance, and j_{HCOOH} per ECSA of the Bi/Cu foam and Bi/Cu foam-*in-situ* treated electrodes.

Sample name	j_{HCOOH} (mA cm^{-2})	C_{dl} (mF cm^{-2})	j_{HCOOH} per ECSA (mA cm^{-2})
Bi/Cu foam	0.08	1.12	0.07*α
Bi/Cu foam-*in-situ treated*	0.45	4.02	0.11*α

The α (mF cm^{-2}) represents the specific capacitance of bismuth.

Table S4 The calculated binding energies (E_{ads}, eV) of various CO_2RR species on Bi(012) and $Bi_2O_2CO_3$(001) facets.

Species	Binding energy (eV)	
	*COOH	*OOCH
Bi (012)	-1.41	-2.33
$Bi_2O_2CO_3$ (001)	-1.77	-3.41

Table S5 Comparison of electrochemical reduction of CO_2 performance for Bi-based catalysts.

Electrocatalyst	Electrolyte	Applied potential (V)	Faradaic effciency (%)	Current density (mA cm^{-2})	Ref
Bi/Cu foam	0.1 M $KHCO_3$	-1.7 V vs. Ag/AgCl (-1.1 V vs. RHE)	92.3	10.29	This work
Bi nanoflakes	0.1 M $KHCO_3$	-0.4 V vs. RHE	79.5	-	Nano Energy, 2017, 39, 44-52.
Bi/BiOCl	0.5 M $KHCO_3$	-1.50 V vs. SCE	92	3.7 mA mg^{-2}	Electrochemistry Communications, 2014, 46, 63-66.
Size tunable nano-Bi	0.5 M $KHCO_3$	-1.60 V vs. SCE	98.4	9.7	Journal of CO_2 Utilization, 2017, 20, 328-335.
Oxide-derived Bi films	0.5 M $KHCO_3$	-0.92 V vs. RHE	82	j_{HCOOH}= 8.3 mA cm-2	Journal of CO_2 Utilization, 2017, 19, 276-283.
Ultrathin Bismuth nanosheets	0.5 M $NaHCO_3$	-1.0 V vs. RHE	Over 90%	12.5	ChemSusChem, 2018, 11, 848-853.
Nano-sized Bi	0.1 M $KHCO_3$	-1.70 V vs. Ag/AgCl	91.3	6	Applied Surface Science, 2017, 393, 191-196
Bi_{45}/GDE	0.5 M $KHCO_3$	-1.45 V vs. SCE	90	4	Applied Catalysis B: Environmental, 2017, 218, 46-50.
P-orbital delocalization (POD)-Bi	0.5 M $KHCO_3$	-1.16V vs. RHE	95	55	Angewandte Chemie International Edition, 2018, 57, 16114-16119.
Bi Dendrite	0.5 M $KHCO_3$	-0.74 V vs. SCE	89	2.6	ACS Catalysis, 2017, 7, 5071-5077.
Lattice-dislocated Bismuth Nanowires/Cu foam	0.5 M $NaHCO_3$	-0.69 V vs. RHE	95	15	Energy & Environmental Science, 2019,12, 1334-1340.
Bi_2S_3-derived Bi	0.5 M $NaHCO_3$	-0.75 V vs. RHE	84	5	Journal of Materials Chemistry A, 2018,6, 4714-4720.

References

1. F. Li, L. Chen, M. Xue, T. Williams, Y. Zhang, D. R. MacFarlane and J. Zhang, *Nano Energy*, 2017, **31**, 270-277.
2. J. P. Perdew, K. Burke and M. Ernzerhof, *Phys. Rev. Lett.*, 1996, **77**, 3865.
3. J. Harl and G. Kresse, *Phys. Rev. Lett.*, 2009, **103**, 056401.
4. A. Klamt and G. Schüürmann, *J. Chem. Soc., Perkin Trans. 2*, 1993, **5**, 799-805.
5. Y. Liu, J. Zhao and Q. Cai, *Phys. Chem. Chem. Phys.*, 2016, **18**, 5491-5498.
6. X. An, S. Li, A. Yoshida, Z. Wang, X. Hao, A. Abudula and G. Guan, *ACS Sustain. Chem. Eng.*, 2019, **7**, 9360-9368.
7. H. J. Monkhorst and J. D. Pack, *Phys. Rev. B*, 1976, **13**, 5188-5192.
8. J. K. Nørskov, J. Rossmeisl, A. Logadottir, L. Lindqvist, J. R. Kitchin, T. Bligaard and H. Jonsson, *J. Phys. Chem. B*, 2004, **108**, 17886-17892.
9. A. A. Peterson, F. Abild-Pedersen, F. Studt, J. Rossmeisl and J. K. Nørskov, *Energy Environ. Sci.*, 2010, **3**, 1311-1315.
10. D.-H. Lim and J. Wilcox, *J. Phys. Chem. C*, 2012, **116**, 3653-3660.
11. S. Kattel, P. Atanassov and B. Kiefer, *J. Phys. Chem. C*, 2012, **116**, 17378-17383.
12. Y. Zhang, X. Zhang, Y. Ling, F. Li, A. M. Bond and J. Zhang, *Angew. Chem. Int. Ed.*, 2018, **57**, 13283-13287.
13. F. Zhang and A. C. Co, *Angew. Chem. Int. Ed.*, 2020, **59**, 1674-1681.